Automatic Control and Navigation

Control of the vehicle is to be automated during the majority of the descent. This phase begins following wing deployment and continues until the start of the landing cycle. The landing sequence will be accomplished through remote control by a ground controller at the recovery site.

Because the vehicle cannot be sighted visually during the initial portion of the descent, it must be flown automatically. A three-axis autopilot will be employed to maintain the proper vehicle attitude. Only when the vehicle has come within sight of the recovery area will it be released to manual control.

The vehicle will be equipped with a long-range navigation system (LORAN), which will be coupled directly to the autopilot. Prior to launch, waypoints are programmed into the LORAN. When the autopilot is activated, the vehicle files a specific descent profile.

Electrical System

An eight-channel receiver is used to control the functions of the flight vehicle. Of the eight channels, four are assigned to the autopilot and primary flight controls. Servomechanisms are used as the actuating mechanisms. During autopilot operation the three primary flight control channels (elevator, rudder, and ailerons) from the receiver are disabled, allowing signals from only the autopilot to activate the servomechanisms. Conversely, when the autopilot is disengaged, the three flight control channels are active. This approach allows only one set of signals to reach the flight controls, either from the autopilot or from the ground controller.

The remaining four channels are assigned to engine start, wing lock release, landing-gear release, and flaps. At the instant of engine start, a timer is activated, and the wing lock is released at a predetermined elapsed time. This serves as a backup feature, allowing wing deployment to occur in the event that no signals are received from the ground controller.

Trajectory Analysis

An analysis of the trajectory was conducted with SORT.[2] This program allows three-dimensional trajectory optimization. Only point-mass trajectories were analyzed. Engine burnout occurs 36 s after liftoff, at an altitude of 12,965 ft. The maximum altitude achieved by the vehicle is 18,870 ft.

Concluding Remarks

This paper indicates that it may be possible to design a simple reusable rocket. The next step will be to build and test such a vehicle. This design could be extended and adapted to larger vehicles in order to attain the higher altitudes that are required in some of the applications of sounding rockets, such as upper-atmospheric experiments.

Acknowledgments

The authors of the design report on which this Note is based deserve the credit for this design. They were the undergraduate design class of the Department of Aerospace Engineering of the University of Alabama in the spring of 1994. The members of the class were James Daniel, Kimberly Kunzweiler, Kazuhiro Nishita, TongSay Vongpaseuth, Bryan Warren, Juan Webb, and Dick Woo.

References

[1]Anon., "Technical Manual, LR101-NA-7," Rockwell International, Rocketdyne Division, Report R-6795-3, Canoga Park, CA, July 1987.

[2]Berning, M. J., and Frick, J. D., "User's Guide for the Simulation and Optimization of Rocket Trajectories (SORT) Program," Lockheed Engineering and Sciences Co., July 1989.

I. E. Vas
Associate Editor

Spacecraft Optimization with Combined Chemical–Electric Propulsion

Craig A. Kluever*
University of Missouri–Columbia/Kansas City, Kansas City, Missouri 64110

Introduction

RECENT research has involved vehicle and mission optimization for electric orbit transfer vehicles,[1–3] and lunar missions have been of specific interest.[4,5] Lunar missions using advanced all-chemical propulsion systems have also been investigated.[6] In this note, vehicle and trajectory optimization of a lunar–interplanetary mission using a combined chemical and electric propulsion system is performed. The mission scenario involves a translunar injection (TLI) from low Earth orbit (LEO) via the upper stage of a Delta II launch vehicle, followed by a lunar orbit insertion (LOI) chemical burn into an intermediate, high-altitude circular lunar orbit, followed by a low-thrust orbit transfer to a polar, circular low lunar orbit (LLO) using electric propulsion. After data are collected at the desired 100-km polar LLO (for instance, lunar gravity mapping), the spacecraft escapes the moon's gravity field using electric propulsion to initiate the interplanetary leg of the two-phase scientific mission. An explicit interplanetary target is not defined, so that the mission analysis can remain general yet at the same time retain the essence of a dual-mission scenario.

The optimization problem involves maximizing the spacecraft's payload for a given fixed launch-vehicle capability and fixed transfer time. The vehicle sizing feature requires computing the optimal chemical burns for TLI and LOI, the optimal electric input power P, and the optimal specific impulse I_{sp} for the electric propulsion stage. The mission design feature involves computing the optimal TLI conditions at LEO and the optimal lunar altitude and inclination for the LOI burn. The latter mission design feature defines how much of the transfer to polar LLO is performed by the chemical and by the electric propulsion stage. The vehicle and mission optimization features exhibit a strong interaction.

Payload and Propulsion-System Analysis

The total mass of a spacecraft with chemical and electric stages after TLI is

$$m_{TLI} = m_{p_c} + m_{dry_c} + m_{p_e} + m_{tank_e} + m_{pp} + m_{net} \qquad (1)$$

where m_p is the propellant mass, m_{dry_c} is the dry mass of the chemical stage, m_{tank_e} is the tank mass of the electric stage, m_{pp} is the power- and propulsion-system mass of the electric stage, and m_{net} is the net mass. The subscripts c and e represent the chemical and electric propulsion stages, respectively. The injected mass m_{TLI} is computed from a linear approximation of the launch performance of a Delta II vehicle[7]:

$$m_{TLI} = -27C_3 + 1227 \text{ kg} \qquad (2)$$

where C_3 is the injection energy (km^2/s^2). The propellant masses m_{p_c} and m_{p_e} are calculated from the rocket equation using the appropriate velocity change ΔV and I_{sp} for the respective maneuver. The specific impulse I_{sp} of the chemical stage is fixed at 310 s. The dry mass m_{dry_c} includes the structural, engine, and tank mass of the chemical stage and is assumed to be 15% of the chemical propellant mass.[6]

Received Sept. 19, 1994; revision received Jan. 12, 1995; accepted for publication Jan. 12, 1995.

*Assistant Professor, Mechanical and Aerospace Engineering Department. Member AIAA.

The tank mass m_{tank_e} is 10% of the propellant for the electric stage.[2] The power- and propulsion-system mass of the electric stage, m_{pp}, is the product of electric input power P and the specific mass α.

Maximum-Payload Problem

The objective of the maximum-payload problem is to maximize the net mass of the spacecraft for a one-way, fixed-time transfer from LEO to polar LLO and on to lunar escape conditions. The full vehicle and mission optimization problem may be divided into two separate trajectory segments: 1) the short-duration, translunar coast phase with two chemical burn maneuvers at each end, and 2) the long-duration low-thrust orbit transfers to polar LLO and from LLO to lunar escape. Since the full optimization problem is numerically intensive, the two trajectory segments are uncoupled, and the translunar coast phase is solved individually. The optimal translunar-phase solutions are used to provide boundary conditions for the subsequent low-thrust orbit transfers.

Optimal Chemical-Stage Maneuvers

The objective is to compute the optimal TLI and LOI chemical burns, which result in the maximum spacecraft mass in a specified high-altitude, inclined circular lunar orbit. The performance index to be maximized is m_{LOI}, the spacecraft mass after the LOI burn and separation of the spent chemical stage. Numerical solutions of the optimization problem are obtained by utilizing sequential quadratic programming (SQP), a constrained parameter optimization method.[8] The SQP design variables include the magnitude and orientation of the velocity vector for TLI at 185-km altitude above Earth, the angular position of the spacecraft at TLI with respect to the Earth–moon line, and the translunar coast time. Two SQP equality constraints are imposed to force the translunar coasting trajectory to terminate at the desired lunar altitude and inclination. At the final time (LOI), the magnitude of the in-plane ΔV required to produce a circular orbit is computed, and the LOI propellant mass is calculated. The initial mass before the LOI burn is m_{TLI} as computed from Eq. (2) and the SQP design variable C_3. The three-dimensional coasting trajectory from TLI to LOI is governed by the dynamics of the classical restricted three-body problem.[9]

A sequence of optimal three-dimensional transfers is obtained for a range of lunar altitudes and inclinations. Altitudes for circular lunar orbit range from LLO (100 km) to the lunar sphere of influence (64,562 km), and inclinations include 0 deg (planar), 45 deg, 90 deg (polar), and 135 deg (retrograde). Figure 1 presents the maximum spacecraft mass after the chemical LOI burn and separation of the chemical stage. Each point represents an optimal transfer to a circular lunar orbit with a fixed inclination and altitude. The optimal injection energy C_3 ranges from -2.5 to -1.8 km^2/s^2, and the corresponding injected mass m_{TLI} ranges from 1295 to 1276 kg. The largest performance penalty is for a chemical LOI into a 100-km circular orbit (LLO). Very little deviation in performance between the different lunar inclinations exists up to a lunar altitude of about 5000 km. The performance levels off for the planar case and peaks for the other inclinations at a circular altitude of about 13,000 km.

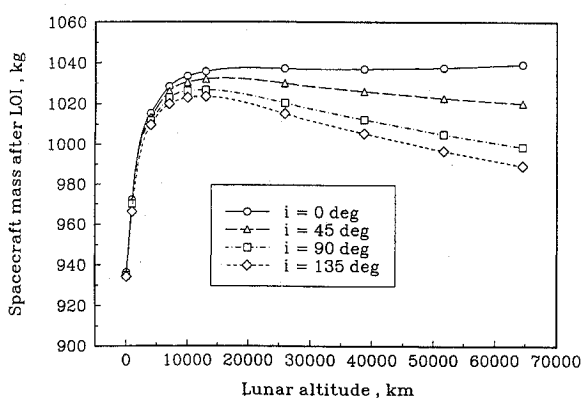

Fig. 1 Optimal spacecraft mass after LOI.

Complete Vehicle and Mission Optimization

The maximum-payload problem for the complete mission scenario is solved numerically using SQP. The SQP performance index to be maximized is the net mass m_{net}, and the four SQP design variables are the input power P and I_{sp} for the electric propulsion stage and the circular lunar altitude and inclination for the initiation of the low-thrust orbit transfer to LLO. Upper and lower constraints of 7000 and 2000 s, respectively, are imposed on the design parameter I_{sp}. A two-dimensional cubic-spline curve fit of Fig. 1 with lunar altitude and inclination as independent variables determines the optimal m_{LOI}. An analytical expression for quasicircular transfers between circular orbits[10] is utilized to approximate the velocity increment for the low-thrust transfer to polar LLO. The rocket equation is utilized to calculate m_{Pel}, the propellant mass required for the transfer to LLO. The low-thrust capture time τ_{capt} is calculated by dividing m_{Pel} by the propellant mass flow rate $\dot{m}$. The mass flow rate is a function of the thruster efficiency η, input power P, and I_{sp}:

$$\dot{m} = \frac{2\eta P}{(gI_{\text{sp}})^2} \tag{3}$$

The thruster efficiency η for ion engines using xenon is determined by an analytic relation using I_{sp} and propellant-dependent coefficients.[5] The design parameters P and I_{sp} are regarded as fixed over the duration of the mission. Equivalently, this assumes a single operating point and no engine throttling. The transfer time τ_{esc} for the escape spiral from polar LLO is computed by scaling universal low-thrust trajectory solutions by the initial thrust acceleration and LLO radius.[11] Finally, the total propellant m_{Pe} for the electric stage is calculated by summing m_{Pel} with the product of τ_{esc} and $\dot{m}$.

Because the maximum-payload problem is solved for a fixed transfer time, the sum of the translunar coast time and the low-thrust transfer times (τ_{capt} and τ_{esc}) must be computed. The coast time from TLI to LOI is calculated by curve-fitting the optimal translunar solutions with altitude and inclination as independent variables. The translunar coast time ranges from 3.7 to 5.9 days for the range of altitudes and inclinations. A single SQP equality constraint requires that the computed total transfer time correspond to the desired fixed transfer time.

Results

Several maximum-net-mass solutions for the complete mission scenario have been obtained for a range of fixed transfer times. Since the SQP problem involves only four design variables and one equality constraint, the solution method is very efficient. Replacing the sensitive translunar coast phase with curve-fit solutions greatly increases the robustness of the solution method.

The optimal net mass fraction $m_{\text{net}}/m_{\text{TLI}}$ for the combined chemical–electric propulsion mission is presented in Fig. 2. Since the optimal injection energy C_3 was observed to be nearly constant at -2 km^2/s^2 for each solution, the injected mass m_{TLI} is approximately 1281 kg for all solutions. The maximum-payload problem is solved for two fixed values of specific mass, $\alpha = 35$ and 25 kg/kW, which represent current and near-term levels in propulsion- and power-system technology, respectively.[3] The optimal payload fraction for an all-chemical mission is approximately 0.55, as shown in Fig. 2. Both maximum-payload curves in Fig. 2 exhibit a steep

Table 1 Maximum-net-mass solutions: $\alpha = 35$ kg/kW

Transfer time, days	P, kW	I_{sp}, s	LOI alt., km	i_{LOI}, deg	τ_{capt}, days	τ_{esc}, days	$m_{\text{net}}/m_{\text{TLI}}$
16	24.5	2000	100	90.0	0	11	0.0
50	6.2	2011	100	90.0	0	46	0.50
100	3.3	2506	100	90.0	0	96	0.59
200	2.9	3234	3399	89.9	60	136	0.65
350	2.2	4135	6050	89.5	124	222	0.69
500	1.8	4882	6526	89.3	180	316	0.71

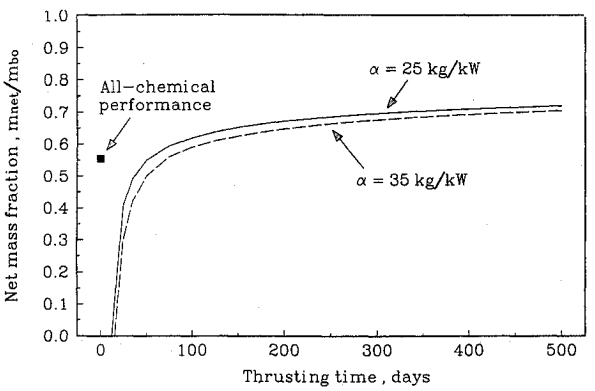

Fig. 2 Optimal net mass fraction.

rise in performance until the transfer time reaches about 75 days. The performance curves level off after about 150 days and approach asymptotic payload fractions of about 0.71 and 0.72 for $\alpha = 35$ and 25 kg/kW, respectively.

A summary of six representative maximum-net-mass solutions for $\alpha = 35$ kg/kW is presented in Table 1. The optimal P, I_{sp}, LOI altitude and inclination, low-thrust capture and escape transfer times, and payload fraction are shown in this table for a range of total transfer time. The optimal translunar injection trajectory results in a nearly polar orbit at LOI for all transfer times. Therefore, very little plane change is performed by the electric stage from LOI to polar LLO. Also, a direct chemical orbit insertion into polar LLO is optimal until the total transfer time is increased past 100 days.

Conclusions

A combined vehicle and mission optimization problem has been formulated and solved for a lunar–interplanetary mission using combined chemical and electric propulsion stages. The complex problem is solved by uncoupling the short-duration chemical insertion translunar phase from the long-duration electric propulsion phases, and the result is a very efficient, robust approach. Several optimal vehicle–mission combinations have been obtained for a range of transfer times from 16 to 500 days. A combined chemical–electric propulsion mission can provide an additional 15% payload capability compared to the corresponding all-chemical mission.

Acknowledgments

This research was funded by NASA Lewis Research Center under Grant NAG3-1650. The author would like to thank Mark Hickman, Steve Oleson, Kurt Hack, Jeff George, and Glen Horvat for their suggestions and contributions to this research project.

References

[1]Burton, R. L., and Wassgren, C., "Time-Critical Low-Thrust Orbit Transfer Optimization," *Journal of Spacecraft and Rockets*, Vol. 29, No. 2, 1992, pp. 286–288.

[2]Oleson, S. R., "An Analytical Optimization of Electric Propulsion Orbit Transfer Vehicles," NASA CR-191129, May 1993.

[3]Oleson, S. R., "Influence of Power System Technology on Electric Propulsion Missions," AIAA Paper 94-4138-CP, Aug. 1994.

[4]Kluever, C. A., and Pierson, B. L., "Vehicle-and-Trajectory Optimization of Nuclear Electric Spacecraft for Lunar Missions," *Journal of Spacecraft and Rockets*, Vol. 32, No. 1, 1995, pp. 126–132.

[5]Gilland, J. H., "Mission and System Optimization of Nuclear Electric Propulsion Vehicles for Lunar and Mars Missions," NASA CR-189058, Dec. 1991.

[6]Palaszewski, B., "Lunar Missions Using Advanced Chemical Propulsion: System Design Issues," *Journal of Spacecraft and Rockets*, Vol. 31, No. 3, 1994, pp. 458–465.

[7]Anon., "Delta II Payload Planner's Guide," McDonnell Douglas Astronautics, Doc. MDC-H3224C, Huntington Beach, CA, Oct. 1993.

[8]Pierson, B. L., "Sequential Quadratic Programming and Its Use in Optimal Control Model Comparisons," *Optimal Control Theory and Economic Analysis 3*, North-Holland, Amsterdam, 1988, pp. 175–193.

[9]Szebehely, V. G., *Theory of Orbits, the Restricted Problem of Three Bodies*, 1st ed., Academic Press, New York, 1967, pp. 7–21.

[10]Edelbaum, T. N., "Propulsion Requirements for Controllable Satellites," *ARS Journal*, Vol. 31, No. 8, 1961, pp. 1079–1089.

[11]Perkins, F. M., "Flight Mechanics of Low-Thrust Spacecraft," *Journal of the Aerospace Sciences*, Vol. 26, No. 5, 1959, pp. 291–297.

J. A. Martin
Associate Editor

Integrated Aerodynamic and Propulsive Flowfields of a Generic Hypersonic Space Plane

Ganesh Wadawadigi* and John C. Tannehill†
Iowa State University, Ames, Iowa 50011
and
Scott L. Lawrence‡ and Thomas A. Edwards§
NASA Ames Research Center, Moffett Field, California 94035

Introduction

A TYPICAL hypersonic space plane is envisioned to be an air-breathing vehicle equipped with a supersonic combustion ramjet (scramjet) engine with hydrogen as its fuel. One of the most important design aspects of the hypersonic space plane is the propulsion-airframe integration. The advantages of such a design in providing increased efficiencies have been well established. The high-Mach-number flight conditions for hypersonic space planes produce strong shocks in the external flowfield and lead to chemical reactions in the air surrounding the vehicle. This, coupled with the complicated combustion processes occurring in the scramjet, makes ground testing of such configurations extremely difficult and expensive. Thus, computational fluid dynamics (CFD) plays an important role in the analysis of the external as well as the internal flowfields of such configurations.

In the present paper, tip-to-tail flowfield calculations of the integrated aerodynamic and propulsive flowfields of the Test Technology Demonstrator[1] (TTD), shown in Fig. 1, have been performed. The TTD has an integrated propulsion airframe geometry which is typical of hypersonic space planes. The flow calculations are performed using an upwind parabolized Navier-Stokes (UPS) code. Two test cases are considered. The first one corresponds to a power-

Presented as Paper 94-0633 at the AIAA 32nd Aerospace Sciences Meeting, Reno, NV, Jan. 10–13, 1994; received Jan. 25, 1994; revision received April 12, 1994; accepted for publication April 13, 1994.

*Graduate Research Assistant, Department of Aerospace Engineering and Engineering Mechanics; currently Research Associate, Center for Hypersonic Research, University of Texas at Arlington, Arlington, TX 76019. Member AIAA.

†Manager, Computational Fluid Dynamics Center and Professor, Department of Aerospace Engineering and Engineering Mechanics. Fellow AIAA.

‡Research Scientist, Computational Aerosciences Branch. Member AIAA.

§Chief, Aerothermodynamics Branch. Senior Member AIAA.